6th International Conference on Silicon Photovoltaics, SiliconPV 2016

High-mobility hydrogenated indium oxide without introducing water during sputtering

Mathieu Boccard*, Nathan Rodkey, Zachary C. Holman

School of Electrical, Computer, and Energy Engineering, Arizona State University, Tempe, Arizona 85287-5706, USA

Abstract

The key role of water to obtain high-mobility IO:H (hydrogenated indium oxide) layers has been well documented, but introducing the required tiny amount of water is technologically challenging. We first use simulations to evidence the key role of high mobility for the transparent conductive oxide for high-efficiency crystalline silicon solar cells. Then, we investigate an approach to fabricate high-mobility IO:H that circumvent the introduction of water vapor, relying on water vapor from ambient air. A sputtering tool equipped with a residual gas analyzer allows partial pressure monitoring of hydrogen and water in the system, and to link the gas composition to the properties of the deposited films. To vary the residual water pressure, we varied the pumping time after opening the chamber and before starting the deposition to reach different base pressures ($1. 10^{-5}$ mbar to $3. 10^{-7}$ mbar), which are mostly composed of residual water. An optimum base pressure around $3. 10^{-6}$ mbar—and not lower pressures—was found to yield the highest mobility values after annealing. An alternative approach by introducing a small flow of hydrogen together with argon and oxygen is also shown to provide promising results.

Keywords: Transparent Conductive Oxide ; Indium Oxide ; Hydrogen ; Reactive Sputtering ; Light Trapping ; .

1. Introduction

Hydrogenated indium oxide (IO:H) is an attractive transparent conductive oxide material since it can achieve mobility values above 100 cm^2/Vs together with a carrier concentration in the 10^{20} cm^{-3} range [1,2,3]. This makes

_____

* Corresponding author. Tel.: +1-480-965-3196; fax: +1-480-965-3196.
   E-mail address: mathieu.boccard@asu.edu

very transparent electrodes for silicon heterojunction solar cells with sheet resistance below 50 $\Omega/\square$. These layers are typically fabricated by sputtering at room temperature from an indium oxide target in an atmosphere of argon, oxygen and water vapor, and subsequently annealing at ~200 °C to induce solid-phase crystallization. The water partial pressure during sputtering was shown by Koida et al. to be crucial to obtain high mobility-films, and should be between 5.10^{-7} mbar and 1.10^{-5} mbar for maximum mobility [1]. Such low partial pressure requires a very small flow which is challenging to control, especially for water vapor which tends to be more difficult to regulate than most other gases.

We first discuss the key role of high mobility to obtain low parasitic absorption in silicon solar cells, using a modified analytical modeling approach based on tracing an average ray of light in the cell. We then present two approaches allowing the preparation of high-mobility indium oxide without water vapor introduction in the vacuum chamber. We first reveal that residual water vapor from opening the chamber can be used as source of water, which quantity can be monitored by measuring the total pressure before introducing gases. Then we show that high mobility values can be obtained even for a low base pressure by introducing oxygen and hydrogen, which is much simpler to control than water vapor.

2. Experimental details

Indium oxide films are prepared by radio-frequency (RF) reactive sputtering from a 75-mm indium oxide target in a single chamber tool equipped with a turbo-molecular pump and three gas lines: Ar, O_2 (10% diluted in Ar) and H_2. It is equipped with a residual gas analyzer allowing to monitor the partial pressures (notably of of H_2, O_2 and H_2O) in the system, and to link the gas composition to the properties of the deposited films. Films are prepared with various compositions and at various base pressures (before introducing any gas) on glass and silicon at room temperature, at a pressure of 8 µbar, and a power of 60W. Deposition time was set to 3 minutes, corresponding to a typical thickness of 130 nm, as measured with spectroscopic ellipsometry. Annealing is performed on a hot plate in ambient air at 230 °C for 20 minutes. Table 1 summarizes the conditions.

Mobility and carrier density values were measured with Hall effect, and the optical properties were measured with spectroscopic ellipsometry, with a Woolam M2000 tool. Absorption curves were extracted from transmission and reflection data which was taken with a Perkin-elmer Lambda 950. These curves were used to improve the uniqueness of the ellipsometry fits.

3. Simulations of the impact of mobility on the optical performance of silicon cells

3.1. Simple optical modeling of crystalline silicon solar cells.

Adapting the formalism developed in [4], an accurate reproduction of both the EQE and R curves of heterojunction solar cells can be made with analytical simulation, especially in the infrared part (Fig. 1a). In addition to reproducing experimental curves, the simulations allow to access non-experimentally-measurable quantities, such as the share of light absorbed parasitically in each layer, as well as the potential gain by suppressing one loss mechanism. Interestingly, the *potential gain* in short circuit current density (Jsc) when suppressing one particular loss mechanism is usually lower than the *calculated loss* in Jsc to this particular mechanism. This is due to the presence of other loss mechanism, which take a share of the light spared from the removed loss mechanism. Similarly to recombination and the leaky bucket analogy, by removing one leak, other leaks will flow more (this comparison has limited validity though: in the case of recombination, all carriers have to be lost to recombination eventually at open circuit, since no carrier is extracted, whereas for photon, not all of them have to be lost and some are usefully absorbed in the wafer). Taking as examples the parasitic absorption of blue light in the front transparent conductive oxide (TCO) layer, light spared from this absorption will partly be absorbed in the silicon wafer (contributing to increased Jsc), but also partly be absorbed in the a-Si:H layer instead (leading to no gain in Jsc). The case of infrared light is similar, though less intuitive to calculate since it involves light trapping and multiple light passes.
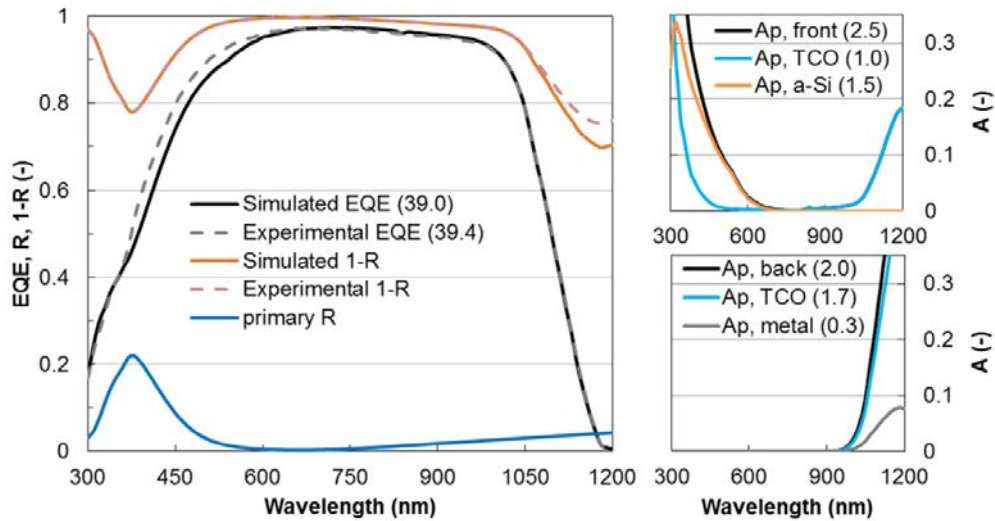
Fig. 1. (a) Experimental and simulated EQE and 1-R curves for a typical silicon heterojunction solar cell as well as primary reflection; (b) calculated parasitic absorption in the front stack of the device, and share absorbed in the TCO and amorphous silicon; (c) calculated parasitic absorption in the rear stack of the device, and share absorbed in the TCO and metal (the amorphous silicon contribution is negligible); All numbers in parenthesis are equivalent current densities when integrating the curve with an AM1.5G spectrum.

Fig. 1b and 1c show the breakdown of parasitic absorption in the front and rear stacks of the device. For the front side, whereas the a-Si:H stack absorbs only UV and visible light, the TCO also contributes some parasitic absorption in the infrared part of the spectrum. For the rear side, absorption in the a-Si:H layers can be neglected and the roles of the TCO and metal are shown. In the particular case shown here, most of the loss is due to the TCO whereas the metal absorption is relatively small, which is attributed to the relatively thick rear TCO. Such modelling allows to identify the lowest hanging fruit in terms of device optical improvement, based on measurable or typical quantities, which are listed in Table 1. In the following, we use this model to discuss the impact of the mobility and carrier density of equally resistive films on the optical performance of silicon cells.

Table 1. Input parameters for optical simulation of the device.

Parameter	Type	Typical value
Wafer thickness	Measured	180 μm
Amorphous silicon layers thickness (i,p)	Measured	4 nm, 11 nm
Front primary reflection	Simulated or Measured (with extrapolation for the >900 nm wavelength range)	
Light path enhancement for the first pass	Simulated	1.3
Light escape fraction for the first pass	Simulated	0.08
Front and rear TCO absorption	Measured	spectrum
Thickness and refractive index around 1200 nm of the rear dielectric	Measured	130 nm / 1.8

3.2. Impact of the mobility and carrier density on optical properties of TCO films for use as electrodes in crystalline silicon cells.

Fig. 2 shows the impact of changing the carrier density and mobility for a constant resistivity on the refractive index and extinction coefficient. A Tauc-Lorentz and Drude combination was used to model one of the experimental films with spectroscopic ellipsometry, and starting from this model, the mobility and carrier density was then varied

(for a constant resistivity) to generate the n, k spectra for different carrier density and mobility couples. As seen from Fig. 2a, low mobility values are detrimental for purpose of front electrode in heterojunction cells in two ways: First, the refractive index drops in the infrared, deviating from the optimal value of ~2 (or higher) for antireflection conditions between air (or encapsulant) and silicon, and second the extinction coefficient in the infrared increases leading to stronger (parasitic) light absorption. Similar observations were made experimentally for ITO in [5].
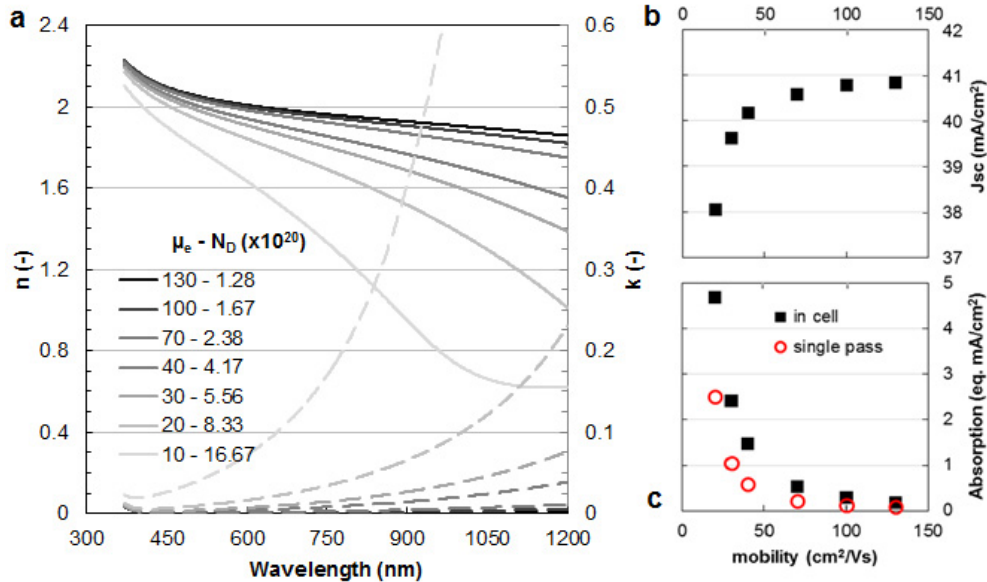

Fig. 2. (a) n and k spectra simulated using a Drude model based on an ellipsometry fit of a reference layer for different mobility (in cm²/Vs) and carrier density values (in cm⁻³) resulting in 3.7.10⁻⁴-Ω.cm-films in all cases; (b) calculated generation current in a silicon heterojunction cell using as front electrode a 75-nm-thick TCO film having different extinction coefficient corresponding to the ones displayed in Fig. 2a; (c) calculated parasitic absorption in these front TCO electrodes for either a single pass or in the cell.

Using these calculated k values, and a 75-nm-thick film (corresponding to a 50 Ω/□ film) the generation current in the silicon heterojunction cell simulated previously was computed and is plotted as a function of the mobility of the films in Fig. 2b. Note that these calculations assume identical primary reflection for all cases, to isolate the role of parasitic absorption losses. Whereas current densities close to 41 mA/cm² are within reach for the high mobility values computed here, it falls softly to 40 mA/cm² when mobility drops to 40 cm²/Vs, and then more steeply to 38 mA/cm² for a mobility of 20 cm²/Vs. Fig. 2c compares the equivalent current density lost to absorption in these typical TCO films in the cell as calculated with the model discussed previously, and the absorption calculated for a single pass as would be measured with a spectrophotometer. Due to light trapping in the cell case, the absorption is larger than for a single pass, and films with a mobility lower than ~50 cm²/Vs result in a detrimentally large absorption to be used in high-efficiency devices. Note that the improvement in calculated Jsc when increasing the mobility of the TCO (Fig. 2b) is smaller than the drop in absorption in the TCO film for the same mobility change because some of the spared light escapes the device or is absorbed in the rear TCO or metal instead.

In the following, we present two approaches to experimentally fabricate high- (>80 cm²/Vs) mobility IO:H without introducing water vapor.

4. Experimental results on IO:H films obtained with no water introduction

High-mobility IO:H films rely on the introduction of small amounts of water during reactive sputtering [1]. To avoid this delicate introduction of water, we investigate the possibility to use water vapor inherently present in the

chamber during pumping. Fig. 3 shows the composition of the ambient in the vacuum chamber right after starting pumping from atmosphere. Whereas most atmospheric gases partial pressure falls below 10^{-6} Torr in a few minutes, water takes much longer to pump and remains in the 10^{-5} Torr range even after an hour. This residual water pressure, detrimental to some processes can be used advantageously for the fabrication of IO:H.
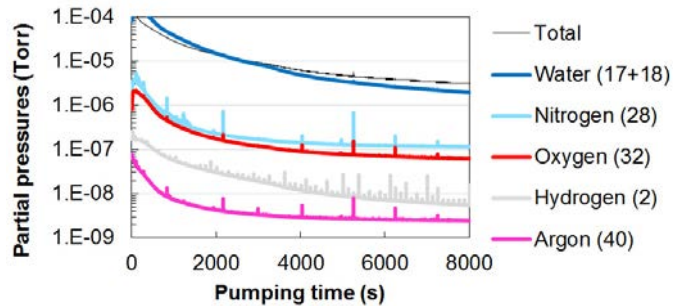

Fig. 3. Partial pressure in the single-chamber sputtering tool used for these experiments as a function of pumping time.
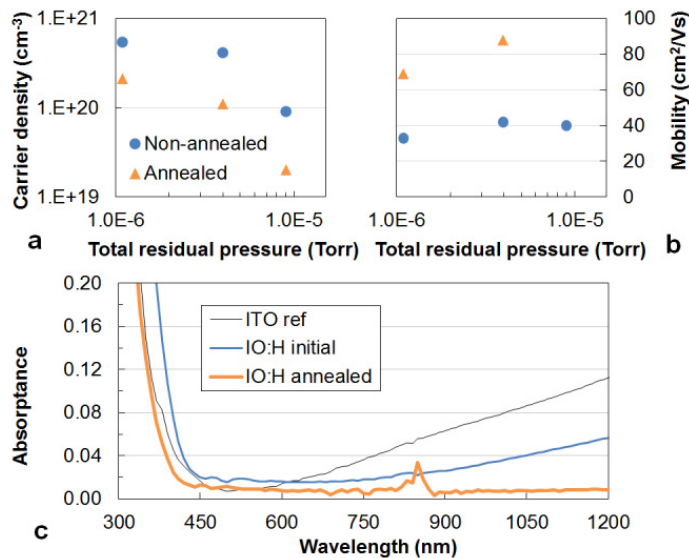

Fig. 4. Carrier density (a) and mobility (b) before and after annealing for IO:H films sputtered with Ar only form an indium oxide target with different pumping times corresponding to different residual pressures in the chamber; (c) Absorptance of the film prepared with a residual pressure of 4.10^{-6} Torr, compared to a typical ITO film.

Fig. 4a and 4b show the carrier density and mobility of IO:H films deposited after different pumping times, corresponding to three different partial pressures in the chamber. The highest mobility value is reached for the film prepared after pumping down to a partial pressure of 4.10^{-6} Torr. Note that the too high resistivity of the film prepared with the highest partial pressure prevented accurate measurement of mobility and carrier density, thus the ellipsometry extracted carrier density value is given.

Fig. 4c shows the absorption before and after annealing of the highest mobility film of the series, compared to a reference ITO film. Even though only Ar was purposefully introduced in the chamber (and neither water or oxygen),

the film shows little absorption over the whole spectrum of interest and especially in the infrared part of the spectrum (< 1%) for a 130-nm-thick film.

Though this process is hardly industrially usable since it implies venting and pumping for long times, the same principle of using atmosphere as a source of water could be extended to higher throughput tools by introducing small amounts of ambient air before processing. Preliminary results using another approach to circumvent the introduction of water through the introduction of hydrogen are shown below.

Fig 5a and b show carrier concentration and mobility before and after annealing of IO:H films prepared with a total residual pressure below 10^{-6} mbar but with various hydrogen partial pressure and a mixture of Ar with 0.2% oxygen as input gas. After annealing, all films exhibit a drop in carrier density to $1\text{-}2.10^{20}$ cm^{-3} and an increase of mobility. For no hydrogen case, the mobility lies between 40 and 60 cm^2/Vs, yet it reaches around 80 cm^2/Vs when 2.10^{-6} Torr of hydrogen is introduced. Increasing further the hydrogen partial pressure, a slight decrease is seen. The carrier density also drops for the largest hydrogen partial pressure, similarly to (though less drastically than) the residual water case. This suggests that hydrogen introduction is a possible alternative method for fabricating high-mobility IO:H without relying on any direct water source. In the range investigated here, all films were transparent indicating no detrimental reduction of the indium oxide.
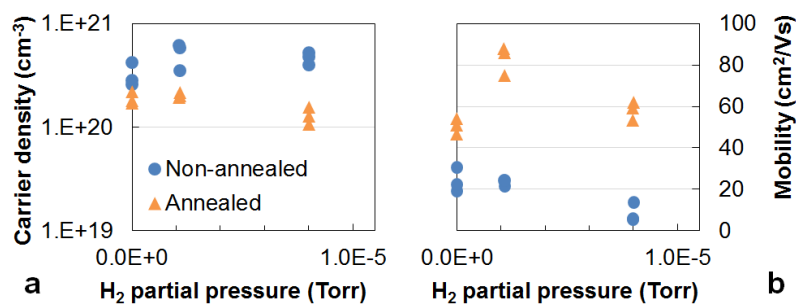

Fig. 5. (a) Carrier concentration and (b) mobility before and after annealing as a function of the hydrogen partial pressure in the chamber.

4. Conclusion

High mobility is the key element to reconcile conductivity and transparency to near-infrared light, allowing for high-efficiency silicon heterojunction solar cells. Parasitic infrared light absorption in the case of low-mobility films is exacerbated in devices compared to single-pass absorption due to light trapping. Based on simulations, we showed that for a typical silicon heterojunction solar cell using a 50-Ω/□ front TCO, layers with mobility values above ~ 50 cm^2/Vs induce little parasitic light loss but these losses increase drastically when mobility is reduced further. Transparent (<1% absorption for the near-infrared range) and high-mobility (above 80 cm^2/Vs) IO:H films were successfully prepared with argon only using residual pressure as water source. Introducing small amounts of hydrogen was shown to be another promising alternative to water vapor introduction during sputtering, a small (but non-zero) hydrogen content was found to be optimal (< 1% of total mix) to obtain highest-mobility films upon annealing.

Acknowledgements

References

[1] Koida T, Fujiwara H, Kondo M. Structural and electrical properties of hydrogen-doped In_2O_3 films fabricated by solid-phase crystallization. Journal of Non-Crystalline Solids 354 (19), 2805-2808 (2008).

[2] Barraud L, Holman ZC, Badel N, Reiss P, Descoeudres A, Battaglia C, De Wolf S, Ballif C. Hydrogen-doped indium oxide/indium tin oxide bilayers for high-efficiency silicon heterojunction solar cells. Solar Energy Materials and Solar Cells. 2013 Aug 31;115:151-6.

[3] Wardenga HF, Frischbier MV, Morales-Masis M, Klein A. In Situ Hall Effect Monitoring of Vacuum Annealing of In2O3: H Thin Films. Materials. 2015 Feb 6;8(2):561-74.

[4] Holman ZC, Filipič M, Descoeudres A, De Wolf S, Smole F, Topič M, Ballif C. Infrared light management in high-efficiency silicon heterojunction and rear-passivated solar cells. Journal of Applied Physics. 2013 Jan 7;113(1):013107.

[5] Boccard M, Battaglia C, Haug FJ, Despeisse M, Ballif C. Light trapping in solar cells: Analytical modeling. Applied Physics Letters. 2012 Oct 8;101(15):151105.